# A Novel β-Defensin Structure: A Potential Strategy of Big Defensin for Overcoming Resistance by Gram-Positive Bacteria[†,‡]

Takahide Kouno,[§] Naoki Fujitani,[||] Mineyuki Mizuguchi,[*,§] Tsukasa Osaki,[⊥] Shin-ichiro Nishimura,[||] Shun-ichiro Kawabata,[⊥] Tomoyasu Aizawa,[@] Makoto Demura,[@] Katsutoshi Nitta,[@] and Keiichi Kawano[@]

*Faculty of Pharmaceutical Sciences, University of Toyama, Toyama 930-0194, Japan, Frontier Research Center for Post-Genomic Science and Technology, Division of Biological Sciences, Graduate School of Science, Hokkaido University, Sapporo 001-0021, Japan, Department of Biology, Kyushu University, Fukuoka 812-8582, Japan, and Division of Biological Sciences, Graduate School of Science, Hokkaido University, Sapporo 060-0810, Japan*

*Received May 21, 2008; Revised Manuscript Received August 22, 2008*

ABSTRACT: Big defensin is a 79-residue peptide derived from hemocytes of the Japanese horseshoe crab. It has antimicrobial activities against Gram-positive and -negative bacteria. The amino acid sequence of big defensin can be divided into an N-terminal hydrophobic half and a C-terminal cationic half. Interestingly, the trypsin cleaves big defensin into two fragments, the N-terminal and C-terminal fragments, which are responsible for antimicrobial activity against Gram-positive and -negative bacteria, respectively. To explore the antimicrobial mechanism of big defensin, we determined the solution structure of mature big defensin and performed a titration experiment with DPC micelles. Big defensin has a novel defensin structure; the C-terminal domain adopts a β-defensin structure, and the N-terminal domain forms a unique globular conformation. It is noteworthy that the hydrophobic N-terminal domain undergoes a conformational change in micelle solution, while the C-terminal domain remains unchanged. Here, we propose that the N-terminal domain achieves its antimicrobial activity in a novel fashion and explain that big defensin has developed a strategy different from those of other β-defensins to suppress the growth of Gram-positive bacteria.

Defensins are polypeptides with antimicrobial activity, and they play a major role in the innate immunity of plants, invertebrates, and vertebrates (*1*−*5*). In terms of the disulfide pattern of defensin molecules, they are classified into four well-known subfamilies: α-defensins, β-defensins, θ-defensins, and insect defensins (*3, 4*). The six half-cystines included in the molecule are linked in the 1−6, 2−4, 3−5 pattern for α-defensin, the 1−5, 2−4, 3−6 pattern for β-defensin, and the 1−4, 2−5, 3−6 pattern for insect defensin. The θ-defensin peptide has a unique circular structure without a free N- or C-terminus, and it is expressed in limited species such as Old World monkeys (*3, 5*). Despite their different disulfide patterns, α- and β-defensin have a similar three-dimensional structure that consists of a triple-stranded β-sheet assisted by three disulfide bonds (*1, 3*−*5*). In addition, both peptides contain many positively charged residues and have a net cationic charge. Because bacteria, the targets of defensins, mainly form their cell membrane with a zwitterionic phosphatidylethanolamine and a phosphatidylglycerol possessing a negatively charged headgroup (*6*), it has been believed that defensins directly bind to the target membranes via electrostatic interactions (*2*−*5*). This idea is supported by the observation that many α- and β-defensins have reduced antimicrobial activities in the presence of a high concentration of salt (*2, 3, 5*). Some groups showed the interaction of defensin with a negatively charged model membrane (*7*−*10*). Although it is not clear how defensin bound to bacterial membranes leads to the death of microorganisms, it has been suggested that defensin forms a transmembrane pore, resulting in permeabilization of the target membrane (*7, 9, 10*). Indeed, Lehrer et al. (*11*) showed that defensin treatment permeabilizes the inner and outer membranes of *Escherichia coli* and then suppresses the bacterial synthesis of DNA, RNA, and protein.

Insect defensin has an α-helix structure in addition to a three-stranded β-sheet; the α-helix and β-sheet structure linked by disulfide bonds is termed the cysteine-stabilized α-helix and β-sheet (CSαβ) motif (*12*). The CSαβ motif is found in the structure of many defensins of insects and plants such as drosomycin (from *Drosophila melanogaster*) and *Raphanus sativus* antifungal peptide (Rs-AFP) (*13, 14*). These defensins act on fungi rather than on Gram-positive and -negative bacteria (*15, 16*). Although the detailed mechanism of fungal growth inhibition remains to be

[†] This study was supported by grants from the Ministry of Education, Culture, Sports, Science and Technology of Japan (MEXT), by the National Project on Protein Structural and Functional Analyses (MEXT), and by the Program for the Promotion of Basic Research Activities for Innovative Biosciences (PROBRAIN).

[‡] The $^1$H chemical shifts and the atomic coordinates of big defensin were deposited in the BioMagResBank as entry 11022 and the Protein Data Bank as entry 2RNG, respectively.

* To whom correspondence should be addressed: Faculty of Pharmaceutical Sciences, University of Toyama, Toyama 930-0194, Japan. Telephone: 81-76-434-7595. Fax: 81-76-434-5061. E-mail: mineyuki@pha.u-toyama.ac.jp.

[§] University of Toyama.

[||] Frontier Research Center for Post-Genomic Science and Technology, Division of Biological Sciences, Graduate School of Science, Hokkaido University.

[⊥] Kyushu University.

[@] Division of Biological Sciences, Graduate School of Science, Hokkaido University.

10.1021/bi800957n CCC: $40.75 
Published on Web 09/12/2008

elucidated, Thevissen et al. (*17*) reported that Rs-AFP directly interacts with a specific glucosylceramide, a membrane component of fungi, and then induces membrane permeabilization.

We have explored the immunity of the Japanese horseshoe crab (*Tachypleus tridentatus*; also called "Kabutogani" in Japanese) and identified a variety of immunity-related factors (*18, 19*). In the horseshoe crab, the hemolymph is responsible for the innate immunity system. The hemolymph is fractionated into hemocytes and hemoplasma. The hemocytes contain two types of granules, large (L) and small (S); degranulation occurs immediately after stimulation, such as the recognition of lipopolysaccharides, outer membrane components of Gram-negative bacteria (*20, 21*). The degranulation leads to a release of many immune factors into the extracellular space. These immune factors include coagulation factors, protein inhibitors, antimicrobial peptides, and lectins that are induced to kill invading microbes and prevent leakage of the hemolymph (*18, 19*).

Big defensin is found in hemocyte granules, both the L and S types, and it has a 79-amino acid sequence with antimicrobial activities against Gram-positive and -negative bacteria and fungi (*22*). Recently, a similar peptide was found in bay scallop *Argopecten irradians* (*23*). The N-terminal half of big defensin is highly hydrophobic, while the C-terminal half includes many positively charged residues. Trypsin cleaves big defensin at the N-terminal side of Arg-37, yielding two fragments, i.e., the hydrophobic N-terminal fragment and the cationic C-terminal fragment (*22*). The C-terminal fragment includes six half-cystine residues linked in the 1−5, 2−4, 3−6 fashion, like $\beta$-defensin. Interestingly, the antimicrobial activities of big defensin can be divided into the two domains; the action against Gram-positive and -negative bacteria is derived from the N-terminal and C-terminal fragments of big defensin, respectively (*22*). To gain structural insight into the antimicrobial activities of big defensin, we resolved the solution structure of a mature big defensin by nuclear magnetic resonance (NMR)[1] spectroscopy. We found that big defensin has a unique structure; it adopts a $\beta$-defensin-like conformation with a hydrophobic globular domain in its N-terminus. These results suggest that big defensin achieves its inhibitory activity against Gram-positive bacteria in a fashion different from those of other $\beta$-defensins.

## EXPERIMENTAL PROCEDURES

*Preparation of Big Defensin.* Big defensin was purified from the Japanese horseshoe crab (*T. tridentatus*) (*22*). Purified big defensin was lyophilized and cryopreserved until further analysis. The purity and the integrity of big defensin were confirmed by reverse-phase high-performance liquid chromatography and mass spectrometry. The peptide concentration was estimated according to the absorbance at 280 nm, and the molar extinction coefficient was based on the number of tyrosine, tryptophan, and half-cystine residues in big defensin ($\varepsilon = 20315\ M^{-1}\ cm^{-1}$) (*24*).

*Circular Dichroism (CD) Spectroscopy.* All CD spectra were recorded on a Jasco J-805 spectropolarimeter with a 1.0 mm quartz cell at 25 °C. Big defensin was dissolved in aqueous buffer [50 mM acetic acid (pH 3.5) and 20 mM NaCl] at a final concentration of 10 $\mu$M. The shape of the CD spectrum of big defensin at pH 3.5 was essentially identical to that at pH 7.0 (data not shown). For titration experiments, the samples contained 0.1−30 mM dodecylphosphocholine (DPC). The CD spectra of all samples were corrected by using reference samples of similarly prepared solutions but in the absence of peptide. Ellipticity was reported as the mean residue molar ellipticity.

*NMR Spectroscopy.* Lyophilized big defensin was dissolved in 250 $\mu$L of aqueous buffer [50 mM deuterated acetic acid (pH 3.5), 20 mM NaCl, and 5 or 100% $D_2O$]. To examine the structure of big defensin in a micellar solution, deuterated DPC (DPC-$d_{38}$) was added at a final concentration of 100 mM. The NMR sample was centrifuged at 15000*g* for 1 min to remove aggregated peptide, and the peptide concentration of the supernatant was estimated to be 0.20−0.25 mM. All of the NMR spectra were acquired at 298 K on Bruker AV600 and AV800 spectrometers equipped with a cryogenic probe. DQF-COSY (*25*), TOCSY (mixing times, 50 and 75 ms) (*26*), and NOESY (80, 100, 120, and 140 ms) (*27*) spectra were acquired with solvent suppression by using the WATERGATE sequence (*28*). DQF-COSY spectra were recorded with 4096 × 512 data points, and the other spectra were recorded with 2048 × 512 data points and 128 scans. $^1$H chemical shifts were directly referenced to the resonance of 2,2-dimethyl-2-silapentane-5-sulfonate sodium salt. The assignments of $^1$H resonances of the backbone and side chains were performed by using a series of two-dimensional NMR experiments as described previously (*29*). The $^3J_{HNH\alpha}$ coupling constants derived from the DQF-COSY spectrum were used for estimation of dihedral angles ($\phi$) according to the Karplus equation. Furthermore, 1 day after big defensin had been dissolved in 100% $D_2O$ buffer, slowly exchanging amide protons were identified from the TOCSY spectrum. All NMR spectra were processed and analyzed with NMRPipe (*30*) and PIPP (*31*).

*Structure Calculations.* For structure calculations of big defensin, distance restraints were collected from two-dimensional homonuclear NOESY spectra acquired with a mixing time of 100 ms in 5 or 100% $D_2O$ buffer. The assignment of NOE cross-peaks and structure calculations was performed iteratively and manually. NOE cross-peak intensities were classified as strong, medium, weak, and very weak, and they were assigned to restraints of 1.8−2.8, 1.8−3.5, 1.8−5.0, and 1.8−6.0 Å, respectively, with appropriate pseudoatom corrections (*29*). The disulfide bond information for Cys-45−Cys-75, Cys-52−Cys-70, and Cys-56−Cys-76 bonds was applied as distance restraints; specifically, the restraints for the Cys $S^\gamma$−Cys $S^\gamma$ and Cys $S^\gamma$−Cys $C^\beta$ distances were set at 2.00−2.10 and 3.00−3.10 Å, respectively. The hydrogen bonds were identified according to amide protons that exchanged slowly with the solvent deuterium, and their partners were assigned on the basis of the early structure calculations. For hydrogen bonds, distance restraints of 2.30−3.30 and 1.30−2.30 Å were used for N−O and HN−O atom pairs, respectively. The restraints for the disulfide and hydrogen bonds and the dihedral angles were incorporated into the late stage of structure calculations.

[1] Abbreviations: CD, circular dichroism; DQF-COSY, double-quantum-filtered correlation spectroscopy; DPC, dodecylphosphocholine; HBD, human $\beta$-defensin; NMR, nuclear magnetic resonance; NOE, nuclear Overhauser enhancement; NOESY, NOE spectroscopy; rmsd, root-mean-square deviation; TOCSY, total correlation spectroscopy.

Table 1: Structural Statistics for the 25 Lowest-Energy Structures of Big Defensin

| | |
|---|---|
| no. of distance restraints | |
| no. of NOE-derived distance restraints | |
| total | 1096 |
| intraresidue | 434 |
| sequential | 246 |
| medium-range | 159 |
| long-range | 257 |
| no. of hydrogen bonds (as restraints) | 31 (62) |
| no. of disulfide bonds (as restraints) | 3 (9) |
| no. of dihedral angle ($\phi$) restraints | 37 |
| X-PLOR energies (kJ/mol) | |
| $E_{total}$ | 131.34 ± 4.10 |
| $E_{NOE}$ | 18.40 ± 2.10 |
| $E_{dihedral}$ | 0.09 ± 0.07 |
| rmsd from idealized covalent geometry | |
| bonds (Å) | 0.001975 ± 0.000089 |
| angles (deg) | 0.5155 ± 0.0051 |
| impropers (deg) | 0.3678 ± 0.0057 |
| Ramachandran plot (%) | |
| most favored | 73.8 |
| additional allowed | 25.5 |
| generously allowed | 0.6 |
| disallowed region | 0.1 |
| pairwise atomic rmsd (Å) | |
| all molecules | |
| backbone heavy atoms | 0.88 ± 0.28 |
| all heavy atoms | 1.48 ± 0.24 |
| well-defined region (residues 4−79) | |
| backbone heavy atoms | 0.49 ± 0.12 |
| all heavy atoms | 1.19 ± 0.12 |

Finally, a simulated annealing protocol was applied by using 12000 steps at a high temperature (1000 K) and 8000 steps for the cooling process. A total of 50 structures were calculated, and the 25 lowest-energy structures were used for calculation of the energy-minimized average structure. The quality of the obtained structure was analyzed with MOLMOL (*32*) and PROCHECK-NMR (*33*). Structural figures were generated with MOLMOL. The detailed experimental data and the structural statistics are summarized in Table 1.

## RESULTS

*Solution Structure of Big Defensin.* We successfully obtained the NMR spectra to analyze and calculate the solution structure of big defensin. Sequence-specific assignments for all backbone amide protons (except for Asn-1) were made by using the two-dimensional TOCSY and NOESY spectra. The assignment of the cross-peaks on the NOESY spectra showed the presence of secondary structure in the big defensin molecule (Figure 1). The consecutive connectivities such as $d_{N\alpha}(i, i + 3)$ and $d_{\alpha\beta}(i, i + 3)$ are typical patterns characterizing the formation of an α-helix. Residues P15−L24 and A27−N34 explicitly indicate formation of an α-helix structure. In addition, the regions of residues A6−A11 and T64−C70 are also expected to adopt a helical conformation. The further assessment of NOE connectivity, including a long-range NOE, reveals the presence of two $\beta$-sheet structures, a two-stranded parallel $\beta$-sheet in the N-terminal region of big defensin, and another four-stranded antiparallel $\beta$-sheet in the C-terminal half (Figure 2). Because no signal was found between these two $\beta$-sheets in terms of NOE derived from backbone protons, they are expected to be noncontinuous as two separated $\beta$-sheets. The TOCSY spectrum acquired in 100% $D_2O$ solution specified many slowly exchanging amide protons, and 49 of the total of 75 amide protons (excluding three prolines and the N-terminal asparagine) remained observable at least 1 day after the peptide was dissolved in $D_2O$ solution. Many of the slowly exchanging amide protons are consistent with secondary structures as suggested by the NOE connectivities (Figures 1 and 2), and 31 hydrogen bonds were selected for the final stage of structure calculation. The other 18 slowly exchanging amide protons are likely to be derived from residues buried in the interior of the big defensin structure.

A total of 1096 NOE-derived distance restraints were collected to determine the solution structure of big defensin (434 intraresidue, 246 sequential, 159 medium-range, and 257 long-range restraints). In addition, the final structure calculation incorporated information from 31 hydrogen bonds (as 62 distance restraints), three disulfide bonds (as nine distance restraints), and 37 dihedral angles ($\phi$), yielding a well-defined structure with a backbone root-mean-square deviation (rmsd) value of 0.49 ± 0.12 Å for residues 4−79 (Figure 3A and Table 1). According to the Ramachandran plot, almost all residues (except for glycine and proline) of the 25 structures with the lowest energy were within the allowable regions. In the selected structures, there were no distance restraints with a violation value larger than 0.30 Å and no dihedral angle restraints with a violation larger than 3°.

The energy-minimized average structure of big defensin is composed of three α-helices (residues 15−24, 27−32, and 67−70, termed α1, α2, and α3, respectively) and two distinct $\beta$-sheets (residues 12−14, 36−38, 43−45, 50−54, 60−63, and 73−79, termed $\beta$1, $\beta$2, $\beta$3, $\beta$4, $\beta$5, and $\beta$6, respectively) (Figure 3B). Strands $\beta$1 and $\beta$2 are parallel, while the other stands are arranged in the $\beta$3−$\beta$4−$\beta$6−$\beta$5 antiparallel fashion, as shown in Figure 2. The structure of big defensin appears to form two separate domains, i.e., the N-terminal domain with the $\beta$1−α1−α2−$\beta$2 fold and the C-terminal domain with the $\beta$3−$\beta$4−$\beta$5−α3−$\beta$6 fold (Figure 3). The C-terminal domain of big defensin largely consists of a bent $\beta$-sheet supported by three disulfide bridges, Cys-45−Cys-75, Cys-52−Cys-70, and Cys-56−Cys-76, which link $\beta$3 and $\beta$6, $\beta$4 and α3, and the $\beta$4−$\beta$5 loop and $\beta$6, respectively. Almost all secondary structures included in the C-terminal domain are fixed to each other through the disulfide bridges; therefore, the C-terminal structure adopts a very compact and well-defined conformation. Thus, the disulfide bonds contribute to the $\beta$-sheet formation of the C-terminal domain of big defensin. The N-terminal domain is also determined with some degree of convergence despite its lack of disulfide bonds. The convergence may be due to hydrophobic interactions involving many hydrophobic residues, including two tyrosines and a tryptophan (Figure 4A). This idea is supported by the observation that the upfield shift was found in some $^1$H resonances of side chains included in the N-terminal domain. For example, the chemical shift values of $^1H^{\gamma 1}$ of Val-30 and $^1H^{\gamma 1}$ of Arg-37 are 0.12 and −0.01 ppm, respectively. These upfield shifts are likely to be caused by the ring current effect of proximal aromatic residues. In the case of the upfield shift of Ile-7 ($^1H^{\gamma 2}$, −0.03 ppm), it appears to be involved not only in the effect of Tyr-8 but also in that of Tyr-65 and Tyr-66 included in the C-terminal domain (Figure 4A). Thus, a hydrophobic core is formed in

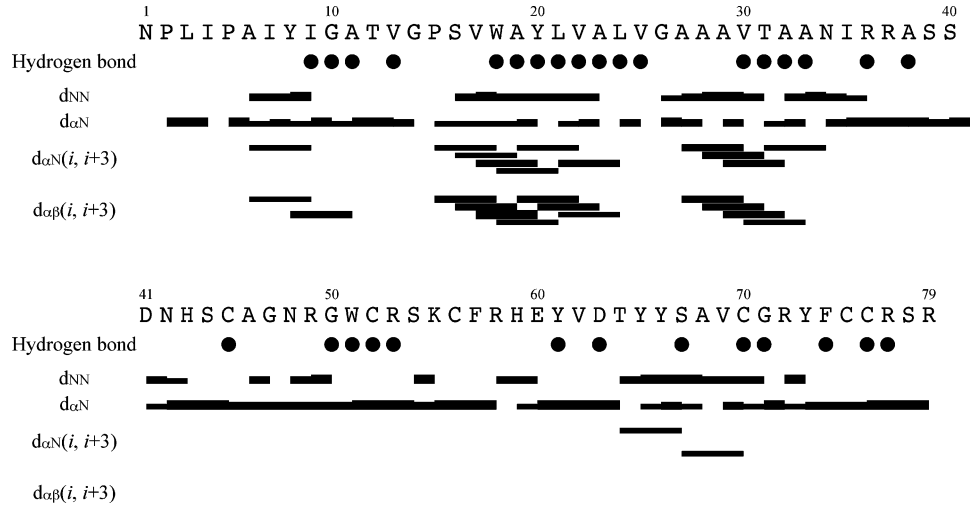


FIGURE 1: Summary of NOE connectivities that are characteristic of the α-helix structure. NOESY spectra were acquired with a mixing time of 100 ms in a 5 or 100% $D_2O$ solution. The thickness of the lines represents the relative intensity of the corresponding NOE cross-peak; e.g., thick lines indicate relatively strong peaks. A dot under the amino acid sequence indicates a slowly exchanging amide proton used as hydrogen bond information in the structure calculation of big defensin.

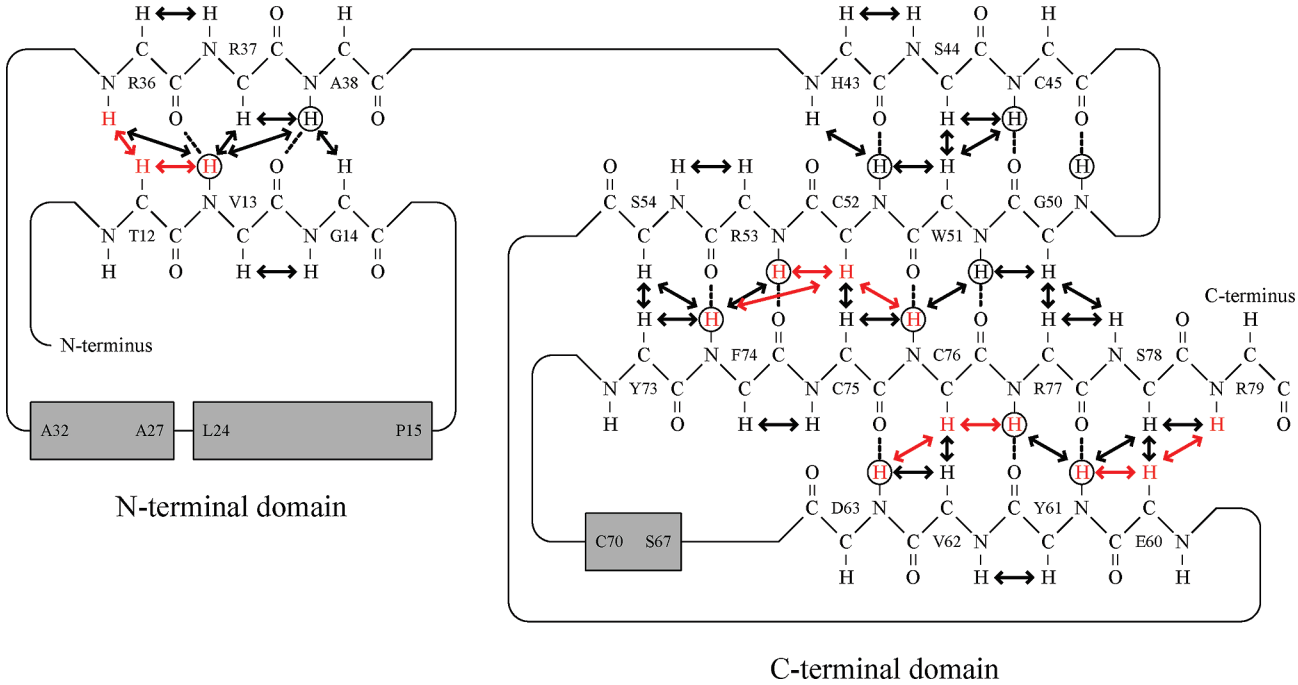


FIGURE 2: Schematic diagram of NOE connectivities that are characteristic of the $\beta$-sheet structure. Observed interresidue NOEs involving HN and $H^{\alpha}$ atoms are shown with double-arrow lines. The red double-arrow lines denote the NOEs mentioned in Figure 5. Amide protons that exchanged slowly with solvent are circled, and the hydrogen bonds used in X-PLOR calculations are shown with broken lines. An α-helix structure is depicted by a shaded rectangle with residues located on the edges.

the N-terminal domain, and it participates in adopting a single compact conformation. Moreover, the N-terminal and C-terminal domains make contacts with each other; therefore, the entire big defensin molecule has a tightly packed structure. Interestingly, two domains of big defensin exhibit a different surface charge distribution; i.e., in contrast to the hydrophobic N-terminal domain, the C-terminal domain of big defensin includes many charged residues and has a cationic net charge (Figure 4B). All charged residues in big defensin are located in the C-terminal domain except for Arg-36 and Arg-37; thus, the overall structure of big defensin has an amphipathic property.

*Structural Change of Big Defensin in Micelles.* To examine the solution structure of big defensin in membrane environments, we acquired the NMR spectra of big defensin in 100 mM DPC-$d_{38}$. The obtained spectra showed a drastic decrease in the number of cross-peaks for the TOCSY experiment and substantial signal overlapping for the NOESY experiment (data not shown). These findings indicate that the addition of DPC leads to a conformational change and/or a dynamic heterogeneity of the big defensin molecule. Fortunately, a part of the fingerprint region of the NOESY spectra gave informative about the solution structure of big defensin in micelles (Figure 5 and Table 2). Although the cross-peak was apparently broadened when DPC was added, the position of signals derived from some residues, such as Cys-52, Glu-60, and Cys-76, remained unchanged. These residues are

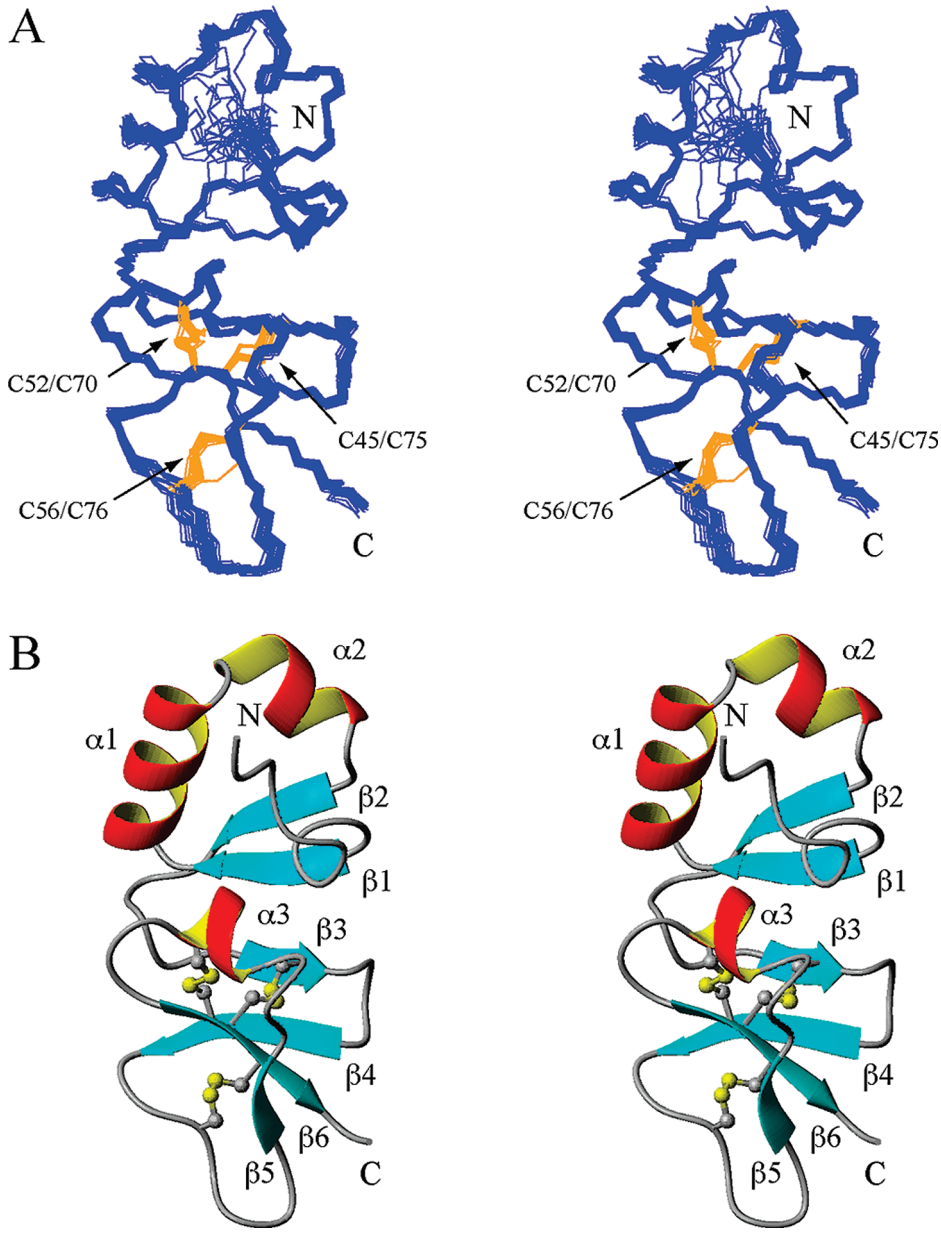


FIGURE 3: Stereoviews of the solution structure of big defensin. (A) Backbone traces of the 25 lowest-energy structures superimposed using the backbone atoms (N, $C^{\alpha}$, and C) of residues 4−79. The side chains of the half-cystine residues and the disulfide bonds are shown with orange lines. (B) Ribbon representation of the energy-minimized average structure of big defensin. The side chains of the half-cystines are shown with a ball-and-stick scheme.

included in the C-terminal $\beta$-sheet of big defensin; for example, Cys-52 and Cys-76 belong to strands $\beta$4 and $\beta$6, respectively (Figure 2). In the NOESY spectrum of big defensin, a cross-peak between $H^{\alpha}$ of Cys-52 and the amide proton of Cys-76 is observed before and after the addition of DPC (Figure 5). This result indicates that the C-terminal antiparallel $\beta$-sheet, at least strands $\beta$4 and $\beta$6, is maintained even in micelles. On the other hand, the NOE cross-peaks between $H^{\alpha}$ of Thr-12 and amide protons of Val-13 and Arg-36 are completely lost after the addition of DPC (Figure 5). Because Thr-12 and Arg-36 are located in strands $\beta$1 and $\beta$2, respectively (Figure 2), the disappearance of the cross-peaks implies that the conformation of the N-terminal $\beta$-sheet is affected by the presence of DPC micelles. This interpretation is also supported by the observation that there is no resonance with a chemical shift value of $<$0.40 ppm in a micellar solution; i.e., the upfield shifts found for Ile-7, Val-30, and Arg-37 are no longer observed. Thus, the NMR experiment with DPC shows different behaviors of the N-terminal and C-terminal domains of big defensin in micelles.

The CD experiments also showed that the conformation of big defensin is altered in a DPC-dependent manner (Figure 6). As DPC was added to the solution, the shape of the CD spectra began to change at a DPC concentration of $>$1 mM, and it reached a plateau at approximately 3 mM. The ellipticity remarkably decreased in the range of 200−240 nm, while the opposite change was found at wavelengths of $<$200 nm. In addition, an explicit isodichroic point at 200 nm is indicative of a gradual transition from a native to another state. Taken together, NMR and CD data imply that DPC induces additional α-helix formation in the N-terminal domain of big defensin.

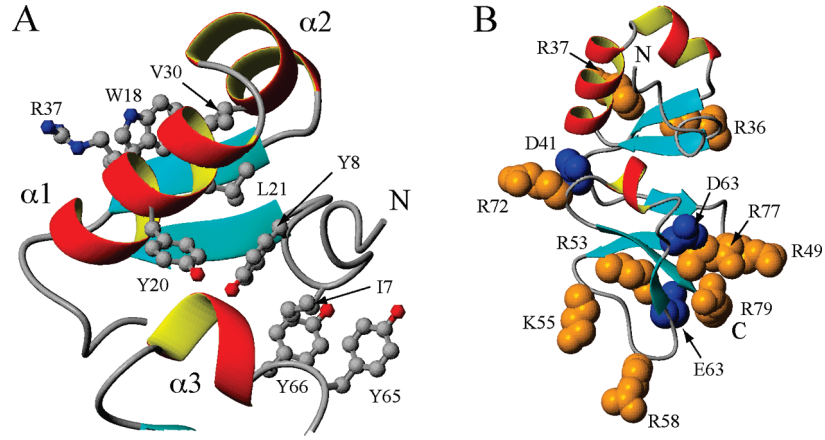


FIGURE 4: Highly hydrophobic N-terminal domain and cationic C-terminal domain of big defensin. (A) Close-up view of the N-terminal domain of big defensin. Residues showing an upfiled shift and the proximal aromatic residues are depicted with a ball-and-stick scheme. A portion of the C-terminal domain is also represented. (B) Charged residue distribution of big defensin. The charged residues are represented in a space-filling model. The positively charged Arg and Lys residues are colored orange, while the negatively charged Asp and Glu residues are colored blue.

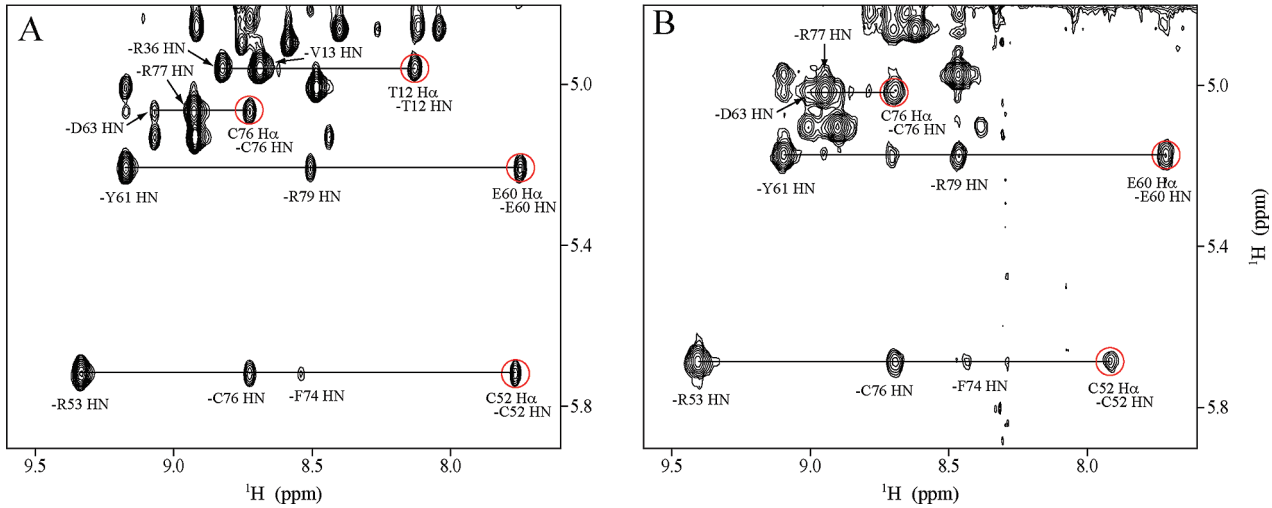


FIGURE 5: Portion of the NOESY spectra of big defensin in the absence (A) and presence (B) of DPC-$d_{38}$. The cross-peak circled in red indicates an intraresidue NOE between HN and $H^{\alpha}$, and their chemical shift values are summarized in Table 2. The horizontal line represents an assignment of NOE cross-peaks; e.g., $H^{\alpha}$ of residue Cys-52 gives cross-peaks with HN groups of Arg-53, Cys-76, and Phe-74. NOE connectivities shown in this panel are also depicted with red double-arrow lines in Figure 2.

Table 2: Chemical Shift Values for the Residues Circled in Figure 5

| | | without DPC | | with DPC | |
|---|---|---|---|---|---|
| residue | domain | $^1H^N$ | $^1H^{\alpha}$ | $^1H^N$ | $^1H^{\alpha}$ |
| Thr-12 | N | 8.13 | 4.97 | no data[a] | no data[a] |
| Cys-52 | C | 7.77 | 5.73 | 7.92 | 5.68 |
| Glu-60 | C | 7.75 | 5.22 | 7.72 | 5.18 |
| Cys-76 | C | 8.73 | 5.08 | 8.69 | 5.01 |

[a] The corresponding signal was not identified because of signal broadening and overlapping.

## DISCUSSION

In this study, NMR-based structure calculations yielded a well-defined solution structure for mature big defensin derived from secretary granules of hemocytes. Although, as a whole molecule, big defensin has a closely packed single-globule conformation, its structure can be divided into the N-terminal domain, including the $\beta1-\alpha1-\alpha2-\beta2$ fold and the C-terminal domain assisted by three disulfide bonds. We searched the Protein Data Bank (PDB) for proteins with structural similarities to the tertiary structure of the N-terminal and C-terminal domains of big defensin by using PAPIA (*34*). As expected, the search with the C-terminal domain found some $\beta$-defensins such as human $\beta$-defensin 2 (HBD2; PDB entry 1FD3) (*35*) and $\beta$-defensin 3 (HBD3; PDB entry 1KJ6) (*36*) (Figure 7). In contrast, a significant structural similarity was not detected between the N-terminal domain of big defensin and any other proteins. Structures of both HBD2 and HBD3 are composed of a three-stranded $\beta$-sheet assisted by three disulfide bonds and an N-terminal short helix. The N-terminal region including the α-helix is linked with the third strand by a disulfide bond; therefore, the $\beta$-sheet of HBD2 and HBD3 lies in the proximity of the N-terminal α-helix. In the structure of big defensin, the region in which HBD2 and HBD3 form the α-helix is replaced by strand $\beta3$, and the C-terminal $\beta$-sheet bends around helix α3 between strands $\beta5$ and $\beta6$ (Figure 7). Despite these differences in global conformation, it is noteworthy that big defensin includes a three-stranded $\beta$-sheet characterizing the $\beta$-defensin fold (*3, 5*). This may reflect the identical disulfide bridge pattern between big defensin and the other $\beta$-defensins. On the other hand, the $\beta1-\alpha1-\alpha2-\beta2$ fold in the N-terminal domain is a unique

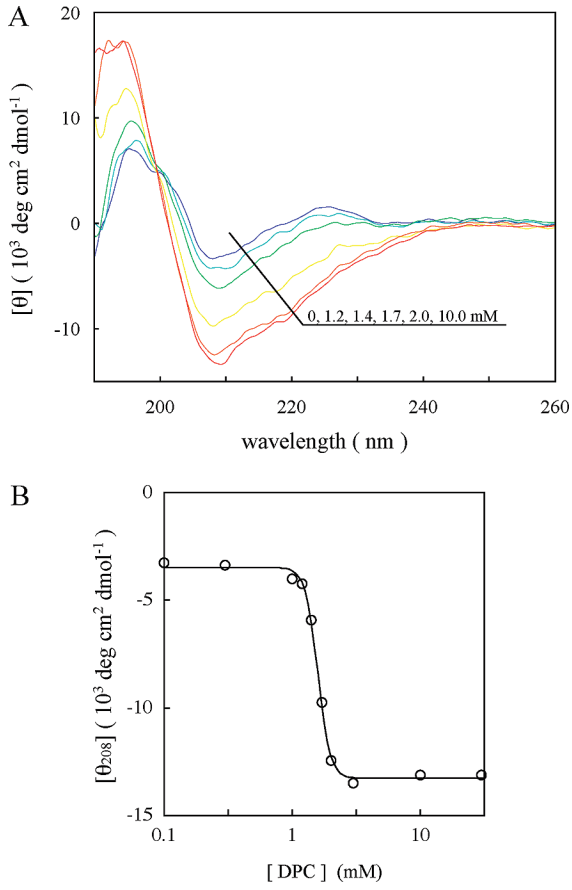


FIGURE 6: Far-ultraviolet CD spectra of big defensin. (A) The CD spectra of big defensin were recorded at various concentrations of DPC at 25 °C. The spectrum at each titration point is shown as a gradual shift from blue (0 mM DPC) to red (10 mM DPC). (B) The titration curve depicted using ellipticity values at 208 nm.

structure; so far, this structure has not been reported for any other $\beta$-defensin. Our NMR studies showed that big defensin is a novel $\beta$-defensin with a hydrophobic globular domain.

We previously showed that the N-terminal and C-terminal domains of big defensin give rise to the antimicrobial activity against Gram-positive and -negative bacteria, respectively (*22*). In other words, the C-terminal domain adopting a $\beta$-defensin fold does not suppress the growth of Gram-positive bacteria but does suppress the growth of Gram-negative bacteria. Like the C-terminal domain of big defensin, human $\beta$-defensin HBD2 effectively kills Gram-negative bacteria, but not Gram-positive *Streptomyces aureus* (*37*). Interestingly, another $\beta$-defensin, HBD3, possesses antimicrobial activity against both types of bacteria (*38, 39*). Schibli et al. (*36*) explained that the increased positive charge enhances the antimicrobial activity of HBD3 against *S. aureus* because HBD3 has a net charge of +11 which is greater than that (+6) of HBD2. Recent studies also showed that the positive net charge and the hydrophobicity of HBD3, rather than a spatial arrangement assisted by disulfide bridges, are indispensable for the antibiotic actions (*40, 41*). These interpretations can apply to the case of big defensin; the C-terminal fragment of big defensin when cleaved by trypsin has a net charge of +5, which is expected to be insufficient for antimicrobial activity against Gram-positive bacteria. In addition, it suggests that big defensin increases its hydrophobicity by incorporating an N-terminal domain to overcome resistance by *S. aureus*. Although a simple charge cannot entirely account for the antimicrobial activity of defensins because the hydrophobic HBD3 fragment with a net charge of +4 also exhibits antimicrobial activity against *S. aureus* (*42*), it is likely that big defensin has developed a unique strategy for suppressing the growth of Gram-positive bacteria.

The two domains of big defensin behave in a different fashion before and after the addition of DPC; the conformation of the C-terminal domain remains unchanged, while the N-terminal domain does not. This difference may be explained by the disulfide bonds in big defensin. The disulfide bonds in the C-terminal domain would restrict the structural perturbation, whereas the structure of the N-terminal domain is not fixed due to a lack of disulfide bonds. On the other hand, the DPC-dependent conformational change of big defensin occurs at a DPC concentration of >1 mM. Considering that the critical micelle concentration of DPC is approximately 1 mM (*43*), the conformational change of big defensin caused by the addition of DPC is expected to be accompanied by the formation of DPC micelles. This interpretation is also supported by a finding that TOCSY and NOESY spectra in the presence of 1 mM DPC are essentially identical to those without DPC (data not shown). DPC is a zwitterionic phospholipid with a positively charged choline group and a negatively charged phosphoryl group. Big defensin has an exclusive distribution of charged residues; i.e., the majority of them are located in the C-terminal domain. When big defensin binds to the DPC micelles, the hydrophilic C-terminal domain preferentially interacts with the charged groups of the DPC molecule. In

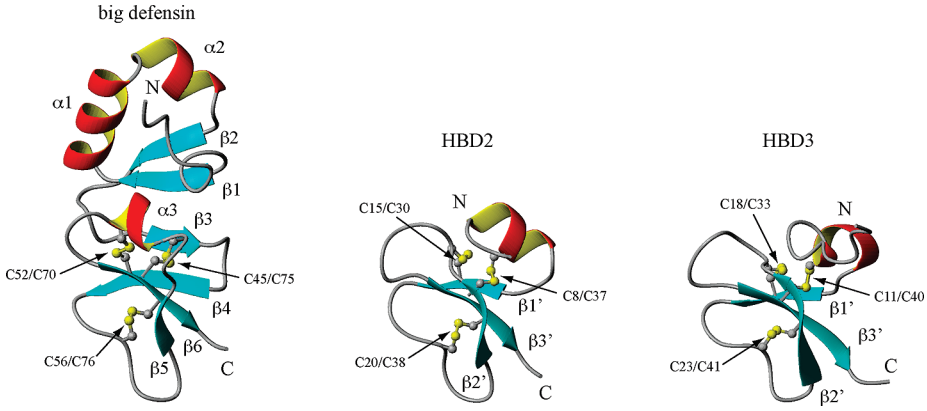


FIGURE 7: Comparison of the three-dimensional structures of big defensin (left), HBD2 (PDB entry 1FD3, middle), and HBD3 (PDB entry 1KJ6, right). The disulfide bridges are shown with a ball-and-stick scheme.

contrast, the N-terminal domain is expected to prefer the interaction with the hydrophobic moiety of the micelle interior rather than with the hydrophilic surface. These situations may be involved in a structural change and/or heterogeneity of the N-terminal domain of big defensin in a micellar solution. Intriguingly, residues Tyr-8−Val-30 included in the N-terminal domain are predicted by using SOSUI (*44*) to form a transmembrane helix structure. These findings imply an insertion of the N-terminal domain into the micelle interior and then an induction of the stronger binding of big defensin to the target membrane through hydrophobic interactions. The participation of hydrophobic interactions in the antimicrobial activity against Gram-positive bacteria is supported by a fact that the big defensin action against *S. aureus* is not affected by the salt concentration in contrast to other defensins (*22*). Most defensins such as HBD2 and HBD3 have an amphipathic property, which contributes to an accumulation of the peptide molecules on the bacterial membrane (*3, 5*). It has been thought that this defensin assembly forms transmembrane "wormholes", resulting in a collapse of the target cell membrane. On the other hand, big defensin achieves the antimicrobial activity against *S. aureus* solely through the hydrophobic N-terminal domain, implying a novel mechanism for killing of Gram-positive bacteria. In addition, we previously reported a synergistic effect in which the action of big defensin on Gram-positive bacteria is enhanced by the other immunity-related factors, tachylectins 5A and 5B (*45*). Although our studies provided the solution structure of big defensin and a potential relationship between the antimicrobial activity and the structural property of the N-terminal domain, the detailed mechanism by which big defensin achieves its antimicrobial activity remains to be determined. Further analysis of big defensin, especially its N-terminal domain, will shed light on the physiological significance of the micelle-induced conformational change and on the unknown mechanism that overcomes resistance to antimicrobial peptides by Gram-positive bacteria.

## REFERENCES


1. Hoffmann, J. A., Kafatos, F. C., Janeway, C. A., Jr., and Ezekowitz, R. A. B. (1999) Phylogenetic Perspectives in Innate Immunity. *Science 284*, 1313–1318.
2. Yang, D., Biragyn, A., Kwak, L. W., and Oppenheim, J. J. (2002) Mammalian defensins in immunity: More than just microbicidal. *Trends Immunol. 23*, 291–296.
3. Ganz, T. (2003) Defensins: Antimicrobial peptides of innate immunity. *Nat. Rev. Immunol. 3*, 710–720.
4. Bulet, P., Stöklin, R., and Menin, L. (2004) *Immunol. Rev. 198*, 169–184.
5. Selsted, M. E., and Ouellette, A. J. (2005) Mammalian defensins in the antimicrobial immune response. *Nat. Immunol. 6*, 551–557.
6. Lohner, K., and Prenner, E. J. (1999) Differential scanning calorimetry and X-ray diffraction studies of the specificity of the interaction of antimicrobial peptides with membrane-mimetic systems. *Biochim. Biophys. Acta 1462*, 141–156.
7. Kagan, B. L., Selsted, M. E., Ganz, T., and Lehner, R. I. (1990) Antimicrobial defensin peptides form voltage-dependent ion-permeable channels in planar lipid bilayer membranes. *Proc. Natl. Acad. Sci. U.S.A. 87*, 210–214.
8. Fujii, G., Selsted, M. E., and Eisenberg, D. (1993) Defensins promote fusion and lysis of negatively charged membranes. *Protein Sci. 2*, 1301–1312.
9. Wimley, W. C., Selsted, M. E., and White, S. H. (1994) Interactions between human defensins and lipid bilayers: Evidence for formation of multimeric pores. *Protein Sci. 3*, 1362–1373.
10. Lohner, K., Latal, A., Lehrer, R. I., and Ganz, T. (1997) Differential scanning microcalorimetry indicates that human defensin, HNP-2, interacts specifically with biomembrane mimetic systems. *Biochemistry 36*, 1525–1531.
11. Lehrer, R. I., Barton, A., Daher, K. A., Harwig, S. S. L., Ganz, T., and Selsted, M. E. (1989) Interaction of human defensins with *Escherichia coli*. Mechanism of bactericidal activity. *J. Clin. Invest. 84*, 553–561.
12. Cornet, B., Bonmatin, J.-M., Hetru, C., Hoffmann, J. A., Ptak, M., and Vovelle, F. (1995) Refined three-dimensional solution structure of insect defensin A. *Structure 3*, 435–448.
13. Landon, C., Sodano, P., Hetru, C., Hoffmann, J. A., and Ptak, M. (1997) Solution structure of drosomycin, the first inducible antifungal protein from insects. *Protein Sci. 6*, 1878–1884.
14. Fant, F., Vranken, W., Broekaert, W., and Borremans, F. (1998) Determination of the three-dimensional solution structure of *Raphanus sativus* antifungal protein 1 by $^{1}$H NMR. *J. Mol. Biol. 279*, 257–270.
15. Fehlbaum, P., Bulet, P., Michaut, L., Lagueux, M., Broekaert, W. F., Hetru, C., and Hoffmann, J. A. (1994) Insect immunity. Septic injury of *Drosophila* induces the synthesis of a potent antifungal peptide with sequence homology to plant antifungal peptides. *J. Biol. Chem. 269*, 33159–33163.
16. Terras, F. R. G., Schoofs, H. M. E., De Bolle, M. F. C., Van Leuven, F., Rees, S. B., Vanderleyden, J., Cammue, B. P. A., and Broekaert, W. F. (1992) Analysis of two novel classes of plant antifungal proteins from radish (*Raphanus sativus* L.) seed. *J. Biol. Chem. 267*, 15301–15309.
17. Thevissen, K., Warnecke, D. C., Francois, I. E., Leipelt, M., Heinz, E., Ott, C., Zahringer, U., Thomma, B. P., Ferket, K. K., and Cammue, B. P. (2004) Defensins from insects and plants interact with fungal glucosylceramides. *J. Biol. Chem. 279*, 3900–3905.
18. Iwanaga, S., Kawabata, S., and Muta, T. (1998) New types of clotting factors and defense molecules found in horseshoe crab hemolymph: Their structures and functions. *J. Biochem. 123*, 1–15.
19. Iwanaga, S. (2002) The molecular basis of innate immunity in the horseshoe crab. *Curr. Opin. Immunol. 14*, 87–95.
20. Toh, Y., Mizutani, A., Tokunaga, F., Muta, T., and Iwanaga, S. (1991) Morphology of the granular hemocytes of the Japanese horseshoe crab *Tachypleus tridentatus* and immunocytochemical localization of clotting factors and antimicrobial substances. *Cell Tissue Res. 266*, 137–147.
21. Chaby, R. (2004) Lipopolysaccharide-binding molecules: Transporters, blockers and sensors. *Cell. Mol. Life Sci. 61*, 1697–1713.
22. Saito, T., Kawabata, S., Shigenaga, T., Takayenoki, Y., Cho, J., Nakajima, H., Hirata, M., and Iwanaga, S. (1995) A novel big defensin identified in horseshoe crab hemocytes: Isolation, amino acid sequence, and antimicrobial activity. *J. Biochem. 117*, 1131–1137.
23. Zhao, J., Song, L., Li, C., Ni, D., Wu, L., Zhu, L., Wang, H., and Xu, W. (2007) Molecular cloning, expression of a big defensin gene from bay scallop *Argopecten irradians* and the antimicrobial activity of its recombinant protein. *Mol. Immunol. 44*, 360–368.
24. Pace, C. N., Vajdos, F., Fee, L., Grimsley, G., and Gray, T. (1995) How to measure and predict the molar absorption coefficient of a protein. *Protein Sci. 4*, 2411–2423.
25. Rance, M., Sørensen, O. W., Bodenhausen, G., Wagner, G., Ernst, R. R., and Wüthrich, K. (1983) Improved spectral resolution in COSY $^{1}$H NMR spectra of proteins via double quantum filtering. *Biochem. Biophys. Res. Commun. 117*, 479–485.
26. Braunschweiler, L., and Ernst, R. R. (1983) Coherence transfer by isotropic mixing: Application to proton correlation spectroscopy. *J. Magn. Reson. 53*, 521–528.
27. Kumar, A., Ernst, R. R., and Wüthrich, K. (1980) A two-dimensional nuclear Overhauser enhancement (2D NOE) experiment for the elucidation of complete proton-proton cross-relaxation networks in biological macromolecules. *Biochem. Biophys. Res. Commun. 9*, 1–6.
28. Sklenar, V., Piotto, M., Leppik, R., and Saudek, V. (1993) Gradient-tailored water suppression for $^{1}$H-$^{15}$N HSQC experiments optimized to retain full sensitivity. *J. Magn. Reson., Ser. A 102*, 241–245.
29. Wüthrich, K. (1986) *NMR of Proteins and Nucleic Acid*, John Wiley & Sons Inc., New York.
30. Delaglio, F., Grzesiek, S., Vuister, G. W., Zhu, G., Pfeifer, J., and Bax, A. (1995) NMRPipe: A multidimensional spectral processing system based on UNIX pipes. *J. Biomol. NMR 6*, 277–293.
31. Garrett, D. S., Powers, R., Gronenborn, A. M., and Clore, G. M. (1991) A common sense approach to peak picking two-, three-

and four-dimensional spectra using automatic computer analysis of contour diagrams. *J. Magn. Reson. 95*, 214–220.
32. Koradi, R., Billeter, M., and Wüthrich, K. (1996) MOLMOL: A program for display and analysis of macromolecular structures. *J. Mol. Graphics 14*, 51–55.
33. Laskowski, R. A., Rullman, J. A., MacArthur, M. W., Kaptein, R., and Thornton, J. M. (1996) AQUA and PROCHECK-NMR: Programs for checking the quality of protein structures solved by NMR. *J. Biomol. NMR 8*, 477–486.
34. Akiyama, Y., Onizuka, K., Noguchi, T., and Ando, M. (1998) Parallel protein information analysis (PAPIA) system running on a 64-node PC cluster. *Genome Inf. Ser. 9*, 131–140.
35. Hoover, D. M., Rajashankar, K. R., Blumenthal, R., Puri, A., Oppenheim, J. J., Chertov, O., and Lubkowski, J. (2000) The structure of human β-defensin-2 shows evidence of higher order oligomerization. *J. Biol. Chem. 275*, 32911–32918.
36. Schibli, D. J., Hunter, H. N., Aseyev, V., Starner, T. D., Wiencek, J. M., McCray, P. B., Jr., Tack, B. F., and Vogel, H. J. (2002) The solution structures of the human β-defensins lead to a better understanding of the potent bactericidal activity of HBD3 against *Staphylococcus aureus*. *J. Biol. Chem. 277*, 8279–8289.
37. Harder, J., Bartels, J., Christophers, E., and Schröder, J.-M. (1997) A peptide antibiotic from human skin. *Nature 387*, 860–861.
38. Harder, J., Bartels, J., Christophers, E., and Schröder, J.-M. (2001) Isolation and characterization of human β-defensin-3, a novel human inducible peptide antibiotic. *J. Biol. Chem. 276*, 5707–5713.
39. García, J. R., Jaumann, F., Schulz, S., Krause, A., Rodríguez-Jiménez, J., Forssmann, U., Adermann, K., Klüver, E., Vogelmeier, C., Becker, D., Hedrich, R., Forssmann, W. G., and Bals, R. (2001) Identification of a novel, multifunctional β-defensin (human β-defensin 3) with specific antimicrobial activity. Its interaction with plasma membranes of *Xenopus* oocytes and the induction of macrophage chemoattraction. *Cell Tissue Res. 306*, 257–264.
40. Klüver, E., Schulz-Maronde, S., Scheid, S., Meyer, B., Forssmann, W.-G., and Adermann, K. (2005) Structure-activity relation of human β-defensin 3: Influence of disulfide bonds and cysteine substitution on antimicrobial activity and cytotoxicity. *Biochemistry 44*, 9804–9816.
41. Taylor, K., Clarke, D. J., McCullough, B., Chin, W., Seo, E., Yang, D., Oppenheim, J., Uhrin, D., Govan, J. R. W., Campopiano, D. J., MacMillan, D., Barran, P., and Dorin, J. R. (2008) Analysis and separation of residues important for the chemoattractant and antimicrobial activities of β-defensin 3. *J. Biol. Chem. 283*, 6631–6639.
42. Hoover, D. M., Wu, Z., Tucker, K., Lu, W., and Lubkowski, J. (2003) Antimicrobial characterization of human β-defensin 3 derivatives. *Antimicrob. Agents Chemother. 47*, 2804–2809.
43. Stafford, R. E., Fanni, T., and Dennis, E. A. (1989) Interfacial properties and critical micelle concentration of lysophospholipids. *Biochemistry 28*, 5113–5120.
44. Hirokawa, T., Boon-Chieng, S., and Mitaku, S. (1998) SOSUI: Classification and secondary structure prediction system for membrane proteins. *Bioinformatics 14*, 378–379.
45. Gokudan, S., Muta, T., Tsuda, R., Koori, K., Kawahara, T., Seki, N., Mizunoe, Y., Wai, S., Iwanaga, S., and Kawabata, S. (1999) Horseshoe crab acetyl group-recognizing lectins involved in innate immunity are structurally related to fibrinogen. *Proc. Natl. Acad. Sci. U.S.A. 96*, 10086–10091.

BI800957N